

Online Estimating State of Health of Lithium-Ion Batteries Using Hierarchical Extreme Learning Machine

Lin Chen^{ID}, Yunhui Ding, Huimin Wang, Yijue Wang^{ID}, Bohao Liu, Shuxiao Wu, Hao Li, and Haihong Pan^{ID}

Abstract—Battery state-of-health (SoH) monitoring is of great importance to ensure the safety and reliability of battery systems. This study proposed an innovative SoH estimation method using hierarchical extreme learning machine (HELM) to improve the estimation robustness and accuracy without the complex parameter model was directly applied to establish the HELM-oriented online SoH estimation framework. First, the increase in mean ohmic resistance was constructed as a novel health indicator (HI) to characterize battery aging. Then, the HI was adopted for offline training to build an HELM model, which captures the underlying correlation between the extracted HI and capacity degradation. Finally, the datasets of four batteries at three different temperatures with dynamic loading profiles were used for validation. The results show that the SoH estimation errors are no more than 1.5%, while the training and estimation datasets are from the same temperature; when the SoH estimation is conducted at different temperatures, the maximum error is only 3.36%. The results indicate that the proposed method had good generalization and reliability for SoH estimation, which is applicable for dynamic scenarios with different temperatures.

Index Terms—Health indicator (HI), hierarchical extreme learning machine (HELM), lithium-ion battery, state of health (SoH).

I. INTRODUCTION

LITHIUM-ION batteries are widely used in electric vehicles (EVs) for energy storage because of their high energy density and long cycle life [1], [2]. To ensure the safety and reliability of power batteries, the battery management system (BMS) is indispensable. The accurate and robust battery state-of-health (SoH) estimation is the core competency of a BMS [3]. SoH determines the period for battery replacement and influences driving mileage. The accurate online SoH

Manuscript received July 19, 2021; accepted August 20, 2021. Date of publication August 24, 2021; date of current version March 22, 2022. This work was supported by the National Natural Science Foundation of China under Grant 52067003 and Grant 51667006. (Corresponding author: Haihong Pan.)

Lin Chen, Yunhui Ding, Bohao Liu, Shuxiao Wu, Hao Li, and Haihong Pan are with the Department of Mechatronics Engineering, College of Mechanical Engineering, Guangxi University, Nanning 530000, China (e-mail: gxdxcl@163.com; yunhuiding05@qq.com; 522719708@qq.com; m13055774581@163.com; 13120506670@163.com; hustphh@163.com).

Huimin Wang is with the School of Mechanical Engineering and Automation, Harbin Institute of Technology, Shenzhen 518000, China (e-mail: wanghmhit@foxmail.com).

Yijue Wang is with the Department of Computer Science and Engineering, University of Connecticut, Storrs, CT 06269 USA (e-mail: yijue.wang@uconn.edu).

Digital Object Identifier 10.1109/TTE.2021.3107727

estimation of lithium-ion batteries is of great significance for ensuring vehicle performance and avoiding accidental battery failure [4].

Generally, when the SoH of the battery falls to the threshold of 80%, this battery is identified as totally aged, and it is no longer applicable to EVs [5]. During the applications of batteries in EVs, many uncertain factors influence the SoH, which makes it difficult to estimate SoH precisely. Thus, accurate SoH estimation is a challenge for the BMS. The development of the SoH estimation methods is critically needed.

A. Review of SoH Prediction Methods

A variety of approaches have been proposed for battery SoH estimation in the existing literature, which can be broadly classified into four categories: 1) direct measurement; 2) model-based; 3) correlation-based; and 4) data-driven approaches.

In direct measurement approaches, the battery SoH is directly calibrated by measured quantities, such as current and internal resistance. The measurement requires the batteries to be tested in static conditions to reduce the errors [1]. Zhang *et al.* [6] presented a model-free SoH calculation method based on the Coulomb counting (CC) to realize the rapid online SoH estimation under the condition of constant current discharge. Galeotti *et al.* [7] introduced a relationship between the ohmic resistance and the available capacity to evaluate the SoH through the electrochemical impedance spectroscopy (EIS) technique. The direct measurement approaches are straightforward and easy to use, but the uncertainty of measurements influences the estimation results and the measurements are time-consuming.

The model-based approaches start with establishing a nonlinear battery degradation model, which is based on the analysis of the degradation process and the equivalent circuit mechanism [8]. The battery SoH is estimated together with degradation model parameters through filter-based algorithms and parameter observers, which aims at improving the adaptability and traceability of the estimation process [9]. Andre *et al.* [10] proposed a dual Kalman filter (KF) based on the second-order RC model to jointly estimate battery state of charge (SoC) and SoH, in which the SoH was calculated from the estimated capacity and ohmic resistance. Tran *et al.* [11] established an autoregressive exogenous model to characterize

the battery degradation, and the dual extended KF was applied to detecting SoH changing. Furthermore, Li *et al.* [12] evaluated the performance of the extended Kalman filter (EKF), least-squares (LS)-based filter, and the particle filter for the impacts of filter configurations and algorithm effectiveness at various aging stages. Kim [13] presented a dual sliding-mode observer to monitor the parameters of the first-order *RC* model and update the resistance and capacity at the same time.

The proposed observer estimated SoH online in terms of capacity fade and resistance deterioration. Besides the filters and observers, Shen *et al.* [14] estimated battery SoH by calibrating capacity from open-circuit voltage (OCV) to SoC table, where the OCV was identified from the Rint equivalent circuit model (ECM) by LS. From the perspective of the ECM, Bian *et al.* [15] described the OCV as a function of the SOC by a polynomial of high degree for SoH estimation based on the Thevenin model. Theoretically, most model-based methods are a closed loop, can achieve high accuracy, and are easy to realize in real time. However, the SoH estimation results are strongly influenced by the precision and robustness of the established battery model, and the computation cost of estimation usually increases as the model accuracy becomes higher.

The correlation-based approaches explore the mapping relationship between specific battery degradation parameters and SoH. The specific parameters mainly adopt the voltage, resistance, and capacitance to represent the degradation of the battery. Liu *et al.* [16] constructed a linear relationship between capacity and the discharging voltage differences in equal time intervals transformed by the Box–Cox transformation. Xiong *et al.* [17] built a correlation function between the solid electrolyte interphase resistance and battery degradation level, and the correlation function was applied to estimate SoH at different discharge rates. Chen *et al.* [18] established a formula based on the estimated diffusion capacitance to calculate the battery capacity. At the same time, the influence of temperature was taken into consideration for improving the robustness of SoH estimation. In addition, the incremental capacity analysis [19] and the differential voltage analysis [20] are also regarded as correlation-based approaches, and they have been extensively used for SoH estimation. These correlation-based approaches take advantage of regression and fitting techniques but hardly take the generalization issue into account.

The data-driven approaches make full use of historical data to process degradation information via advanced machine learning (ML) methods for data analysis, such as an artificial intelligence-based method, time series-based method, and statistical data-driven method. You *et al.* [21] proposed a backpropagation neural network (BPNN) framework that adopted the dynamic historical distributions of collected data to trace the variation of SoH. The traditional BPNN is a kind of local search optimization method, but the results may fall into a local minimum, which leads to the singularities in estimation error. Lin *et al.* [22] employed the constant current charging time, the instantaneous voltage drops at the beginning of discharging, and OCV as the input of probabilistic neural network (PNN) to realize SoH estimation, which can reduce

the error rate and avoid local minimum via the Bayesian decision. The support vector machine (SVM) can construct a linear regression function in high-dimensional feature space using the kernel function, which needs fewer data samples compared with the neural network. Nuhic *et al.* [23] proposed an SVM-based method with the combination of load collectives and the coherent capacity tests. The SoH estimation was validated by real driving cycles. The optimization of the hyperparameters in SVM can significantly reduce the generalization error, but it can be a time-consuming effort. For this issue, Yang *et al.* [24] presented the least-square SVM (LS-SVM) method for SoH estimation with a simpler solution procedure and faster running speed, in which the particle swarm optimization was introduced to optimize the hyperparameters. Also, it is clear that the learning speed has been the bottleneck of the feedforward neural networks' applications to get good generalization performance and fast learning speed. Pan *et al.* [8] introduced the ELM to capture the underlying correlation between the extracted health indicators (HIs) and capacity degradation to improve the speed and to acquire the accuracy of ML for online estimation. In order to settle the problems of gradient disappearance and gradient explosion in neural networks, Qu *et al.* [25] proposed a new data-driven combined long short-term memory (LSTM) with particle swarm optimization for the SoH monitoring, and the results show that the presented method has higher accuracy. Actually, there are too many parameters that need setting in the LSTM neural network. Richardson *et al.* [26] used gated recurrent unit (GRU) neural networks for the SoH prediction. Compared to LSTM, the GRU algorithm has slightly higher estimation errors while needing fewer parameters (about 25% fewer). Statistical data-driven method is a nonparametric method. Ungurean *et al.* [27] utilized the Gaussian process regression (GPR) to forecast battery SoH. It can model complex systems and approach the uncertainty in a principled manner. The superiority of these data-driven approaches is that the mechanism of battery degradation is unnecessary, and only external characteristic data of the battery are required. Furthermore, these approaches showed good performance in nonlinearity and adaptability, and satisfactory results can be obtained with sufficient training data [1]. Nevertheless, the accuracy of data-driven methods is significantly dependent on the quantity of training data, and the parameter tuning for the estimation algorithms is complex work. These are two issues that need to be further researched and addressed.

B. Contributions of the Study

In this article, we propose an innovative viewpoint that combines the correlation-based idea and the data-driven approaches for overcoming the drawbacks of the data-driven approaches while achieving high accuracy of SoH estimation. The key contributions are summarized as follows.

- 1) *An HI Definition:* The increase of mean ohmic resistance (MOR) in one discharging cycle was extracted as an HI. The HI from different cycles could represent the degradation process of the battery, and they could help reduce the category and quantity of training data. The HI

extraction method was rapid and easy to realize online because it used the identification method of recursive LS with a forgetting factor (FFRLS) for the Thevenin model. The HI was insensitive to the polarization effect caused by dynamic loading profiles, and it could reduce the random disturbance from loading conditions via data averaging. Besides, mapping relationship between HI and capacity could be established.

- 2) *A Hierarchical Extreme Learning Machine (HELM)-Oriented SoH Estimation Framework:* HELM has the superiorities of fast learning speed and good generalization due to the randomly generated and tuning-free parameters in hidden layers [28]. The HELM is working as the data-driven algorithm and the extracted HI as an input parameter to capture the mapping relationship between the HI and battery capacity. The innovative SoH estimation framework is constructed for offline HELM training and online SoH estimation. This framework could avoid complex parameter-tuning issues. The generalization ability of the HELM can ensure the robustness for the synergy of offline and online parts. In addition, the HELM algorithm is a regression method with simplicity, less time-consuming, and easy to implement. When it was used in the BMS system, the online estimation process will occupy fewer resources to achieve the purpose of fast estimation.
- 3) *Robustness and Universality for Application:* Because of the effectiveness of the HI and generalization of HELM, high accuracy of estimation could be achieved even if only one kind of HI and short data were used during training and estimation. An established mapping relationship between the HI and capacity via HELM was reliable and universal, and it was verified by dynamic aging tests of different batteries. Specifically, for the same battery, the well-trained relationship model trained under one loading profile could be applicable for SoH estimation under other different loading profiles. Experimental results showed that the proposed method could achieve accurate and robust SoH estimation in the EVs working conditions over different temperatures and dynamic loading conditions.

C. Arrangement of the Study

The remainder of this article is organized as follows. First, the experimental tests and HI extraction are given in Section II. Then, in Section III, the HELM theory is introduced, and the HELM-oriented framework is proposed for SoH estimation. In Section IV, the comparative results of SoH estimation are shown, and error analysis is conducted. Finally, the conclusions and future work are discussed in Section V.

II. EXPERIMENTAL DESIGN

A. Battery Testing Systems

An experimental test bench was designed to facilitate the research on battery SoH (Fig. 1). The test bench includes lithium-ion batteries, a dc charger ITECH IT6532D, an electronic load ITECH IT8511 A+ in Table I, an environmental

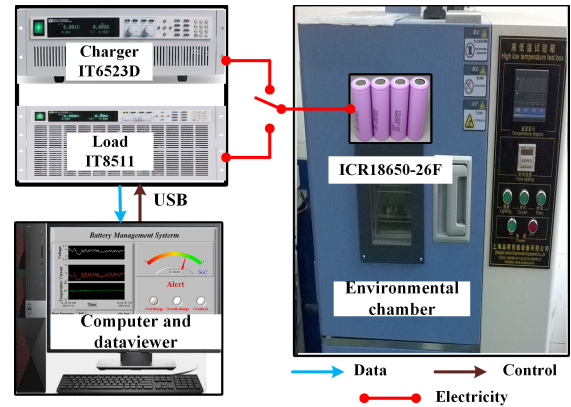


Fig. 1. Experimental test bench.

TABLE I
MAJOR EQUIPMENT PARAMETERS OF CHARGER AND LOAD

Device name	IT6523D	IT8511 A+
Maximum voltage (V)	160 V \pm 0.2% FS*	120 V \pm 0.05% FS
Maximum current (A)	120 A \pm 0.2% FS	30 A \pm 0.1% FS
Voltage accuracy (V)	\pm (0.05%+5mV)	\pm (0.05%+0.02% FS)
Current accuracy (A)	\pm (0.1%+10mA)	\pm (0.05%+0.05% FS)

FS*= Full Scale

chamber GDW-100L, some custom switching circuitries, and a computer for user-machine interface and data storage.

Four batteries of commercial Samsung lithium cobalt oxide (LiCoO_2) ICR18650-26F with 2.6-Ah nominal capacity were used for the test. They were labeled as No. 17, No. 30, No. 42, and No. 43. The data of voltage, current, and temperature were collected with a 1-Hz sampling rate. All tests were conducted in the environmental chamber under predetermined temperatures.

B. Battery Test Schedule

Two series of different tests were designed and conducted successively to investigate battery degradation.

1) *Test A:* No. 17 and No. 30 were loaded and degraded through three different test profiles, including a capacity step, a discharge step, and an aging step at 35 °C. The tests were carried out repeatedly until 20% capacity loss was achieved (considered as the end of life). More experimental details are referred to [8].

2) *Test B:* No. 42 and No. 43 test schedules were designed to investigate the batteries' characteristics and aging (Fig. 2). The aging test generated dynamic degradation, which considered EV environments in a more practical means. The entire tests mainly consist of two parts.

III. METHODOLOGY

A. Model Parameters Identification and HI Extraction

Methods based on ECM are one of the mainstream methods in battery state estimation, in which the first-order RC model

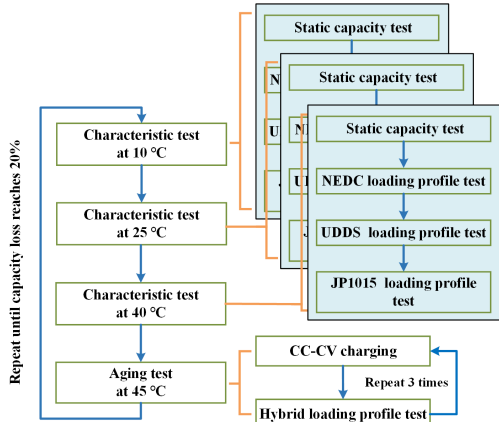


Fig. 2. Battery test schedule for No. 42 and No. 43.

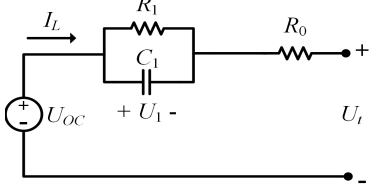


Fig. 3. Thevenin model.

has better generalization ability than the other ECMs [29]. Thus, we employed the first-order RC model, also known as the Thevenin model, for battery modeling. The parameters of the model (R_0 , R_1 , C_1 , and U_{oc}) were identified by the FFRLS algorithm when the value of U_t and I_L are measured.

The Thevenin model is composed of a voltage source (U_{oc}), an RC network ($R_1//C_1$), and an ohmic resistance (R_0) (Fig. 3). U_{oc} represents the OCV of the battery. R_1 and C_1 are the polarized resistance and polarized capacitance, respectively, which quantitatively describes the polarized characteristics and diffusion effects. Also, R_0 is the ohmic resistance of the battery, which usually comprises the inner resistance of the separator and the contact resistance (resistance of the electrolytes, electrode materials, and other components) [30].

The electrical behavior of the Thevenin model is given by (2) and (3)

$$U_t = U_{oc} - I_L R_0 - U_1 \quad (1)$$

$$I_L = \frac{U_1}{R_1} + C_1 \frac{dU_1}{dt} \quad (2)$$

where U_t represents the terminal voltage, U_1 represents the voltage across the RC network, and I_L is the load current.

Using the Laplace transform, z transform, and discretization, (1) can be expressed as

$$U_{t,k}^i = (1 - \theta_1)U_{oc,k}^i + \theta_1 U_{t,k-1}^i + \theta_2 I_{L,k}^i + \theta_3 I_{L,k-1}^i \quad (3)$$

where k is the sampling time and i denotes the i th cycle

$$\begin{cases} \theta_1 = -\frac{T_s - 2R_1^i C_1^i}{T_s + 2R_1^i C_1^i} \\ \theta_2 = -\frac{R_0^i T_s + R_1^i T_s + 2R_0^i R_1^i C_1^i}{T_s + 2R_1^i C_1^i} \\ \theta_3 = -\frac{R_0^i T_s + R_1^i T_s - 2R_0^i R_1^i C_1^i}{T_s + 2R_1^i C_1^i} \end{cases} \quad (4)$$

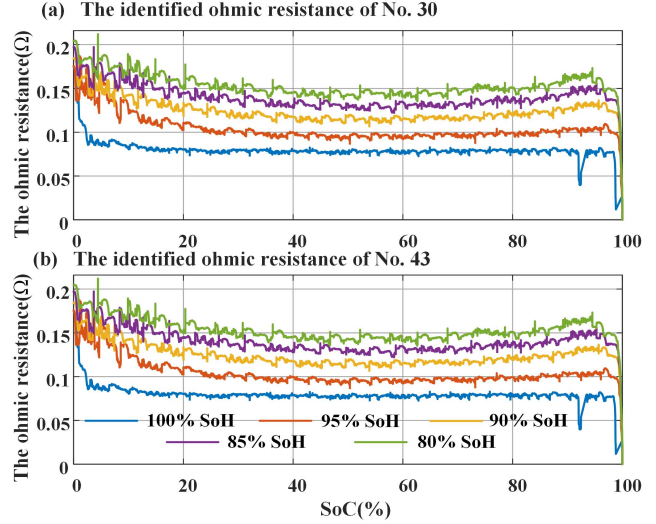


Fig. 4. Trajectories of identified ohmic resistance in different SoHs of (a) No. 30 and (b) No. 43.

where T_s is the sampling period and it is set to 1 second in this article.

For the identification process, the regression form of (3) can be written as

$$U_{t,k} = \Phi_k \Theta_k \quad (5)$$

where $\Phi(k)$ and $\theta(k)$ are the data matrix and parameter matrix, defined by

$$\Phi_k = [1 \ U_{t,k} \ I_{L,k} \ I_{L,k-1}] \quad (6)$$

$$\Theta_k = [(1 - \theta_1)U_{oc,k} \ \theta_{1,k} \ \theta_{2,k} \ \theta_{3,k}]^T. \quad (7)$$

The parameters U_t and I_L in (6) can be obtained by direct measurements, and thus, the data matrix Φ_k is known. Based on the initialization of covariance, the parameter matrix Θ_k in (7) is solved by the FFRLS. The recursive process of FFRLS is given by

$$\begin{cases} \Theta_k = \Theta_{k-1} + K_k [U_{t,k} - \Phi_k \Theta_{k-1}] \\ K_k = \frac{P_{k-1} \Phi_k^T}{\Phi_k P_{k-1} \Phi_k^T + \mu} \\ P_k = \frac{P_{k-1} - K_k \Phi_k P_{k-1}}{\mu} \end{cases} \quad (8)$$

where μ is the forgetting factor, and it is set to 0.95 in this work. P_k and K_k are the covariance matrix and gain matrix at the k th sampling time. After Θ_k is obtained from (8), the model parameters R_0 , R_1 , C_1 , and U_{oc} can be calculated by (3), (4), and (7).

The datasets of No. 30 (NEDC profile) and No. 43 (JP1015 profile) were chosen to validate the FFRLS method and the accuracy and robustness of the model (Table II and Fig. 4). The root-mean-square error (RMSE), mean absolute error (MAE), intervals, and $P_{under-1\%}$ [the proportion of under-1% absolute errors (AEs)] are used to describe the error performance from multiple perspectives. The error intervals between measured terminal voltage and the identified terminal voltage for No. 30 and No. 43 are in different SoH. The error intervals are

TABLE II
ERRORS OF IDENTIFIED TERMINAL VOLTAGE FOR NO. 30 AND NO. 43

SoH	No. 30 (mV) @35°C			No. 43 (mV) @10°C			No. 43 (mV) @25°C			No. 43 (mV) @40°C		
	Intervals	MAE	RMSE									
100%	[-5, 5]	2.1	16.1	[-5, 5]	4.8	24.3	[-5, 5]	4.6	24.1	[-5, 5]	1.4	13.3
95%	[-5, 5]	2.4	16.7	[-5, 5]	5.1	23.4	[-5, 5]	3.6	14.1	[-5, 5]	3.8	21.0
90%	[-5, 5]	2.6	17.6	[-10, 10]	7.2	26.8	[-5, 5]	4.6	23.5	[-5, 5]	3.7	21.4
85%	[-5, 5]	2.7	17.5	[-15, 15]	7.4	26.3	[-5, 5]	4.2	22.6	[-5, 5]	4.0	22.6
80%	[-5, 5]	3.0	18.9	[-15, 15]	8.1	27.9	[-5, 5]	4.3	23.5	[-5, 5]	4.0	22.4

stabilized at $[-5, 5]$ mV at 25 °C, 35 °C, and 40 °C. However, the error intervals are obviously increased with the decline of SoH at 10 °C. This phenomenon reflects the instability of battery voltage at low temperatures. Nevertheless, the upper limit of terminal voltage errors is less than 15 mV (0.55% of cutoff voltage, better than the 1% benchmark in [31]). The maximum MAE of No. 30 and No. 43 is less than 3.0 and 8.1 mV, respectively. The RMSE of them is no more than 27.9 mV, which indicates the good agreement between the measured voltage and identified voltage. It proves that the combination of the Thevenin model and the FFRLS algorithm can accurately track the dynamic changes of batteries under various loading conditions and at different temperatures.

The identified ohmic resistances are used to explore their correlation with battery SoH. Their changing trajectories with SoH reduction have similar trends (Fig. 4). The determined ohmic resistance increases with the decrease of SoH, despite some local fluctuations. This also confirms the conclusion in [32] that there is a negative correlation between impedance and capacity degradation. Different from the EIS, the identified ohmic resistances are easy to calculate and used onboard.

The identified ohmic resistances of No. 43 change more frequently than those of No. 30 because No. 43 introduces the complex hybrid loading profile for its aging (Fig. 4). The changes of identified ohmic resistances fluctuate sharply and irregularly at the beginning and end of discharging, but they are relatively stable most of the time. Our previous work [8] has pointed out that the batteries in EVs mainly work under conditions of 25%–95% SoC in practical use.

The MOR for 30%–80% SoC is applied to approximately describe the real ohmic resistance for certain aging stages in terms of the application scenario, which is described as follows [8], [33]:

$$R_0^i = \frac{1}{n} (R_0(\text{SoC} = 30\%) + \dots + R_0(\text{SoC} = 80\%)) \quad (9)$$

where R_0^i is the MOR of the i th test cycle, $R_0(\text{SoC})$ is the identified ohmic resistance at particular SoC, and n is the number of collected $R_0(\text{SoC})$ data in 30%–80% SoC. The SoC is calculated by the Coulomb-counting method.

The MORs of No. 30 (35 °C) and No. 43 (25 °C) under three loading profiles in different SoH are calculated and shown in Fig. 5. When the SoH changes from 95% to 80%, the MOR increases by 0.05 Ω, which indicates that the SoH conditions influence the values of ohmic resistance significantly. However, when the batteries are at the same SoH condition,

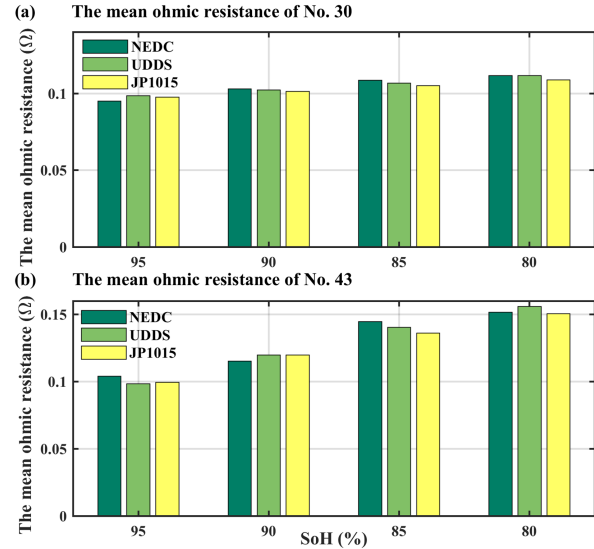


Fig. 5. MOR of (a) No. 30 and (b) No. 43 under three profiles with different SoHs.

TABLE III
MOR FOR NO. 30 AND NO. 43 AT DIFFERENT TEMPERATURES (Ω)

SoH	No. 30		No. 43	
	35°C	10°C	25°C	40°C
100%	0.0772	0.0897	0.0782	0.0756
95%	0.0976	0.1340	0.0996	0.0852
90%	0.1014	0.1683	0.1200	0.0981
85%	0.1051	0.1893	0.1361	0.1067
80%	0.1089	0.2071	0.1503	0.1132

the MORs values for the three loading profiles are similar. Their differences are relatively small, such as the differences are only 0.003 Ω for No. 30 and 0.006 Ω for No. 43. Thus, it is valid to consider that various loading profiles have no significant impact on the calculation results of MOR. In other words, the values of MOR under different loading profiles are the same.

From Table III, it can be seen that at the different temperatures under the same SoH and JP1015 loading profile, the values of MOR vary in a wide range. To efficiently deal with these resistance data for more accurate SoH estimation, a method with better generalization is needed. It is necessary to find a standardized and effective indicator of battery degradation quantification. Thus, the increase in MOR of different

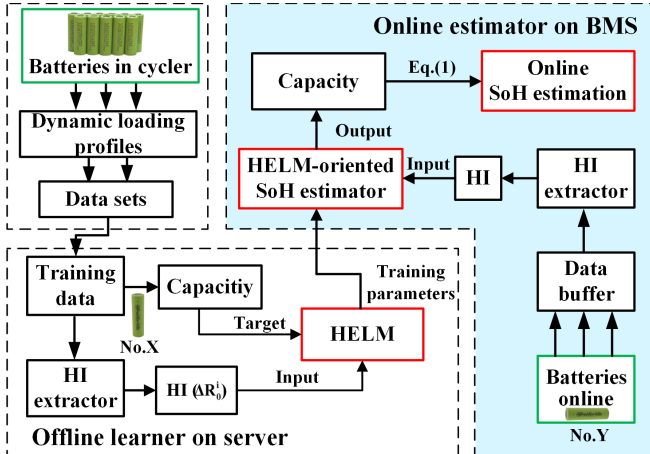


Fig. 6. Flowchart of SoH estimation framework.

cycles is proposed as HI, and it is defined as

$$\begin{cases} \Delta R_0^i = R_0^i - R_0^1 \\ \Delta C^i = C^i - C^1 \end{cases} \quad (10)$$

where ΔR_0^i is the increase in MOR of the i th test cycle, R_0^1 denotes the increase in MOR of the first cycle, C^1 denotes the capacity of the first cycle, C^i is the capacity of the i th test cycle, and ΔC^i is the degradation capacity of the i th test cycle. The proposed HI has three advantages compared with capacity: 1) it can be got online easily, quantify the degradation, and reflect the different degradation processes of lithium-ion batteries; 2) it is not sensitive to the polarization effect caused by the dynamic loading profile and has good robustness; and 3) it can efficiently deal with these resistance data at different temperatures for more accurate SoH estimation, although the values of MOR vary in a wide range.

B. SoH Estimation Based on HELM

The HELM algorithm with good generalization and high computing efficiency is introduced for HI (the increase in MOR) and SoH estimation at dynamic loading conditions. The entire framework of the proposed battery SoH estimation method consists of two main parts (Fig. 6): an offline learner and an online estimator.

In the offline part, the training data take advantage of the datasets collected in advance from batteries in the testing cycler. The voltage and current data are adopted for HIs extraction by parameter identification, and then, the HIs (the increase of MOR) are employed as input to train an HELM model whose target is the corresponding capacity data. The parameters of the well-trained HELM model are obtained after the training. In the online part, the HELM-oriented SoH estimator on BMS accepts the HELM model parameters from the offline learner to establish an online estimation model. By adopting HI extracted from online battery data, the online estimator could trace the battery capacity and SoH on board.

The fundamental theory of HELM is addressed as follows. The ELM (Table IV) is a unique algorithm based on the

TABLE IV
NUMERICAL PROCESS OF ELM

Step 1. Suppose the mathematical representation of ELM with L hidden nodes is

$$\sum_{i=1}^L \beta_i g(\omega_i \cdot \mathbf{x}_j + b_i) = y_j, \quad j = 1, 2, \dots, N$$

where the input is $\mathbf{x}_j \in R^n$ and the desired output is $y_j \in R^m$, b_i represents the random bias of the i -th hidden node, and β_i denotes the output weight that connects the i -th hidden layer nodes and the output layer.

Step 2. Change the equation into a linear form $\mathbf{H}\beta = \mathbf{y}$

$$\text{where } \mathbf{H} = \begin{bmatrix} g(\omega_1 \cdot \mathbf{x}_1 + b_1) & \cdots & g(\omega_L \cdot \mathbf{x}_1 + b_L) \\ \vdots & \cdots & \vdots \\ g(\omega_1 \cdot \mathbf{x}_N + b_1) & \cdots & g(\omega_L \cdot \mathbf{x}_N + b_L) \end{bmatrix}, \quad \beta = [\beta_1, \beta_2, \dots, \beta_L]^T,$$

$$\mathbf{y} = [y_1, y_2, \dots, y_N]^T.$$

Step 3. The target is transformed to finding the optimal solution of the output weight by $\hat{\beta} = \mathbf{H}^+ \mathbf{y}$ where the \mathbf{H}^+ is the Moore-Penrose generalized inverse of \mathbf{H} .

Step 4. The least square and the ridge regression are employed to calculate the output weight $\hat{\beta} = (\mathbf{H}^T \mathbf{H} + \frac{1}{\lambda})^{-1} \mathbf{H}^T \mathbf{y}$

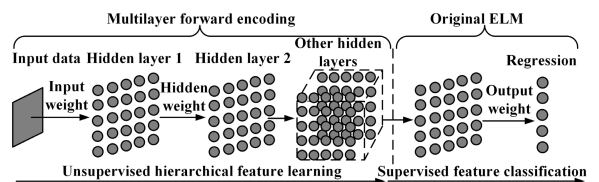


Fig. 7. Entire framework of HELM.

single-hidden layer feedforward neural network. It was proposed by Huang *et al.* [34] and had attracted broad attention in the past few years because of its good generalization and high training speed. Unlike other traditional NNs, the parameters of the hidden layer in ELM are initialized randomly, and there is no need to adjust the input weights and biases. Thus, the hidden layer nodes can be determined before getting the training data. It has been proven that the output weights generated randomly and adjusted by regularized LSs can ensure the approximation ability well [28], [35].

The HELM [36] is built in a multilayer manner, and its architecture can be structurally divided into two main parts (Fig. 7): 1) an unsupervised hierarchical feature learning part and 2) a supervised feature classification part. The former part can extract multilayer sparse features from input data by developing an ELM-based autoencoder. For the latter one, the sparse features from the former part are discussed by original ELM-based regression for decision-making.

Before the unsupervised feature learning, the raw data should be transformed into a random feature space that can extract hidden information from input training samples. To obtain the high-level sparse features, multilayer unsupervised learning is implemented. The output of hidden layers can be represented in mathematics as

$$\mathbf{H}_i = g(\mathbf{H}_{i-1} \beta), \quad i \in [1, K] \quad (11)$$

TABLE V
FISTA ALGORITHM

Step 1. Calculate the Lipschitz constant γ of the gradient of a smooth convex function ∇p .
Step 2. Take $y_0 = \beta_0 \in R^n$, $t_0=1$ as the initial values, then the following equations are tenable for j ($j \geq 1$):
(a) $\beta_j = s_\gamma(y_j)$, $s_\gamma = \arg \min \left\{ \frac{\gamma}{2} \left\ \beta - \beta_{j-1} - \frac{1}{\gamma} \nabla p(\beta_{j-1}) \right\ ^2 + q(\beta) \right\}$
(b) $t_{j+1} = \frac{1 + \sqrt{1 + 4t_j^2}}{2}$
(c) $y_{j+1} = \beta_j + \left(\frac{t_{j-1}}{t_{j+1}} \right) (\beta_j - \beta_{j-1})$
Step 3. Compute the iterative steps above to recover the data.

where \mathbf{H}_i and \mathbf{H}_{i-1} are the output of the i th and $(i-1)$ th hidden layer, respectively, β denotes the output weights, and $g(\cdot)$ is the activation function of the hidden layers. The weights and biases of the current hidden layer will be fixed once the features of the previous layer are extracted.

The ELM-based autoencoder for feature extraction and learning is optimized by the sparse constraints, so it is termed ELM sparse autoencoder. The input weights of ELM sparse autoencoder are determined by searching the path back from a random space. It has been proven that fine-tuning is not required once the autoencoder is initialized by employing the ELM concept. To establish the ELM sparse encoder, the optimization model is proposed as

$$O_\beta = \arg \min \{ \|\mathbf{H}\beta - \mathbf{X}\|^2 + \|\beta\|_{\lambda_1} \} \quad (12)$$

where \mathbf{H} is the random mapping output of ELM, \mathbf{X} denotes the input data, and β is the hidden layer output weight to be calculated. The object function (12) can be rewritten as (13) to describe the λ_1 optimization problem

$$O_\beta = p(\beta) + q(\beta) \quad (13)$$

where $p(\beta) = \|\mathbf{H}\beta - \mathbf{X}\|^2$, $q(\beta) = \|\beta\|_{\lambda_1}$, and λ_1 is the penalty factor of the model.

To solve the optimization problem, the fast iterative shrinkage-thresholding algorithm (FISTA) [37] is implemented (Table V). FISTA improves the selection of the starting point of approximate function in the iterative process, so it achieves faster iterative speed, which makes it approach the minimum function more quickly in the iterative process based on the idea of gradient descent.

In brief, FISTA can achieve as good results as other L1-regularization term solving methods in a shorter time. Also, one important characteristic of HELM is the random assignment of weights and bias, which can speed up the training process. Combining with FISTA, HELM can keep the advantage of fast training.

The resultant base β is used as the weight of the autoencoder, and the inner product of the input data and learned features can reflect the original data. In this way, higher level feature representations are generated by layerwise comparison, and the number of neural nodes can be reduced.

Accordingly, the HELM takes full advantage of the universal approximation capability of ELM. The hierarchical structure and FISTA optimization can help realize higher learning accuracy and better classification performance.

As a typical case for the proposed framework (Fig. 6) in practical application scenarios, the offline training part can be finished in advance on a host computer. For instance, the coding for the adequately trained HELM can be written using the computer and then be debugged and downloaded to the microcontroller units in the BMS via a controller area network bus. Due to the simplification of the HELM network structure by the FISTA algorithm, both offline training and online estimation can be completed at a faster speed, which is more beneficial to the practical vehicle environment.

IV. RESULTS AND DISCUSSION

To verify the advantages of the proposed HELM-oriented estimator, SoH estimation based on HELM is carried out using the three temperatures datasets for universality validation. Furthermore, online SoH estimation is implemented and compared with contrastive ML algorithms.

A. HELM-Oriented SoH Estimation at Same and Different Temperatures

The batteries in real EVs usually work in complex conditions with different temperatures. Temperature is one of the major factors that influenced the battery's available capacity [38]. The proposed HI increases markedly as the temperature decreases (Section II). Hence, the affections of the alteration HI under different temperatures on the SoH estimation accuracy of the HELM are studied in this section.

The whole lifetime tests of No. 17 and No. 30 are conducted at 35 °C (Section II-B). These datasets are used to verify the accuracy of the HELM-oriented SoH estimation framework for estimation of each other, such as the data of No. 30 that is used as the training data for estimating the SoH of No. 17 [Fig. 8(a)]. No. 42 and No. 43 are exhaustively tested by characteristic tests at 10 °C, 25 °C, and 40 °C (Fig. 2). Their datasets are employed for SoH estimation at the same temperature [Fig. 8(b)–(d)], and the range of HI changes with different temperatures. With the decrease of temperatures, the scope of HI increases and for cross estimation at different temperatures (Fig. 9).

The SoH estimation at the same temperature, the true and estimated SoH of No. 17, degrades consistently as the HI increases at 35 °C [Fig. 8(a)]. The error curve shows that the maximum error is no more than 1.6%, and most of the SoH estimation errors are below 1% (Table VI). Although the degradation trajectories of No. 43 are different at 10 °C [Fig. 8(b)], 25 °C [Fig. 8(c)], and 45 °C [Fig. 8(d)], the estimated SoH trajectories still keep good traceability using the data of No. 42 for training. This indicates that two batteries (belong to the same type) tested at the same temperature can predict each other with good accuracy and robustness using the HELM framework.

The SoH estimation at different temperatures: the training data are No. 43 battery at 25 °C and the test data are No. 43

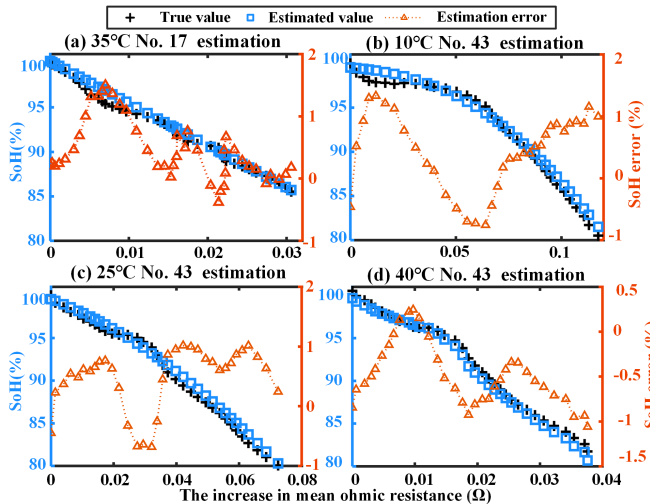


Fig. 8. SoH estimation results at the same temperature. (a) 35 °C: No. 17 estimation by training No. 30. (b) 10 °C: No. 43 estimation by training No. 42. (c) 25 °C: No. 43 estimation by training No. 42. (d) 40 °C: No. 43 estimation by training No. 42.

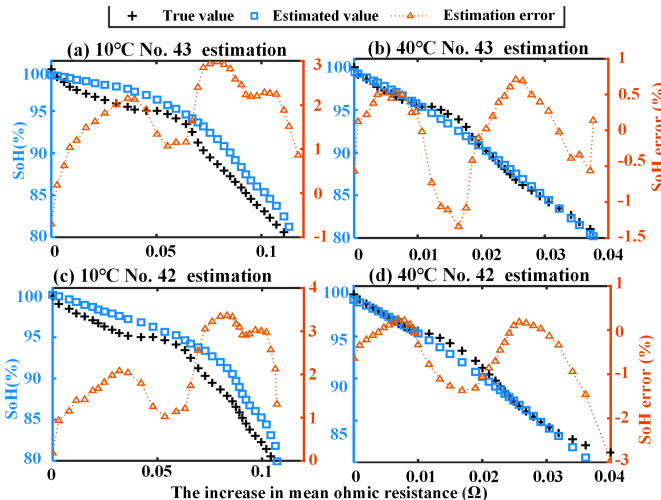


Fig. 9. SoH estimation at different temperatures: results for No. 42 and No. 43 at 10 °C and 40 °C by training No. 43 at 25 °C. (a) 10 °C: No. 43 estimation. (b) 40 °C: No. 43 estimation. (c) 10 °C: No. 42 estimation. (d) 40 °C: No. 42 estimation.

and No. 42 at 10 °C and 40 °C. The SoH estimation results of No. 42 and No. 43 at 40 °C have high fitting precision [Fig. 9(b)–(d)] except for the last estimation value of No. 42. However, the estimated values of No. 42 and No. 43 at 10 °C deviated from the true data, and the local deviations are relatively obvious [Fig. 9(a)–(c)]. Correspondingly, the RMSE at 10 °C is significantly larger than others, and most of their AEs are greater than 1%. As the temperature decreases, the low-kinetics electrochemical reactions take place in various electrochemical processes on electrolyte, electrodes, and solid electrolyte interface (SEI), which contributes to the low lithium-ion transfer rate [39]. Due to the reduction of internal performance, the degradation trajectory of the battery at low temperature is quite different from that at normal temperature. However, if the training data are from 10 °C,

TABLE VI
SOH ESTIMATION ERRORS OF HELM AT SAME AND DIFFERENT TEMPERATURES

Estimation conditions		Maximum AE (%)	MAE (%)	RMSE (%)	$P_{\text{under-1\%}}^*$
Training sample					
No. 30 @35°C	No. 17 @35°C	1.47	0.72	0.7882	89%
No. 42 @10°C	No. 43 @10°C	1.33	0.67	0.7460	85%
No. 42 @25°C	No. 43 @25°C	1.02	0.65	0.6913	97%
No. 42 @40°C	No. 43 @40°C	1.11	0.57	0.3754	97%
No. 43 @25°C	No. 43 @10°C	2.98	1.85	1.9819	21%
	No. 43 @40°C	1.34	0.47	0.5629	88%
No. 42 @10°C		3.36	2.16	2.3235	12%
No. 42 @40°C		2.95	0.54	0.8131	79%

$P_{\text{under-1\%}}^*$: the proportion of under-1% absolute errors

the SoH estimation can obtain satisfactory results, such as the MAE that is only 1.33%, the AEs under 1% account for 85% (Fig. 8(b) and Table VI). This means that HELM can obtain accurate estimation results in most cases by training data only from 25 °C, and the reliable SoH estimation at low temperature can also be realized with the corresponding training data.

Table VII shows the comparison of the direct measurement approaches (such as CC, OCV, and EIS) and model-based approaches (such as EKF and LS) to verify the advantages and performance of the proposed method (HELM). The Maximum AE of CC method is 1% (under the 3C discharge at 40 °C), which is the same as the maximum AE 1.11% of HELM method (under the condition of No. 43 at 40 °C with the dataset of No. 42 at 40 °C as training sample Table VI). The EIS method was tested from 5 °C to 45 °C to take the temperature into account for SoH estimation, but its maximum AE is up to 3.73% and higher than the maximum AE of HELM (3.36%). The KF method has the advantages of accurate and filtering high degree of noise. The RMSE of KF method is 4.6%, but larger than those of HELM at 25 °C. When the testing sample and training sample are at the same temperature, the maximum AE is no more than 1.47% (Table VI), which is less than the five methods (Table VII). These analyses indicate that the HELM has a good performance for SoH estimation.

B. SoH Estimation Using Different ML Algorithms

For comparison, the HELM, traditional BPNN, LS-SVM, and GPR are applied for SoH estimation. The training sample is data from No. 42 at 25 °C, and the testing samples are data from No. 43 at 10 °C, No. 43 at 25 °C, and No. 43 at 40 °C. The configurations of the four algorithms are listed in Table VIII, and the training time was also obtained by running each algorithm 20 times and calculating the average (the time of optimization was not counted). The comparative results are plotted in Fig. 10 and are summarized in Table IX.

The SoH estimation trajectories of GPR and LS-SVM at 10 °C [Fig. 10(a)] and 40 °C [Fig. 10(c)] deviate from the true SoH obviously, but HELM and BPNN still show good traceability. This phenomenon indicates that HELM and BPNN have better reliability when the training sample and testing sample have different input characteristics. The maximum

TABLE VII
COMPARATIVE ANALYSIS FOR SoH ESTIMATION METHODS

Method	Refs.	Conditions	Strength	Weakness	Estimated error
CC	Zhang et al. (2020) [6]	3C discharge at 40°C	Simplicity, Low computational complexity, Low power consumption	Calibration is required after charge/discharge cycle	MAE=0.36%, RMSE=0.44% AE=1%
EIS	Galeotti et al. (2015) [7]	1C discharge at 5-45°C	Avoids complex calculation when using the standalone method	Offline, Processing Specific current patterns, Vulnerable to temperature	AE=3.73%
EKF	Li et al. (2018) [12]	1/6C discharge at 20°C	Accurate, can filter high degree of noise	High computational complexity	RMSE=4.6% AE=4%
LS	Li et al. (2018) [12]	1/6C discharge at 20°C	Low algorithm complexity, Short execution time	Need time for improving the controller	RMSE=5%
OCV	Bian et al. (2021) [15]	0.3C discharge at 0°C and 0.5C for acceleration	Easy to implement	Cannot operate online	AE=2.9%

* The five methods were both charged with CC-CV.

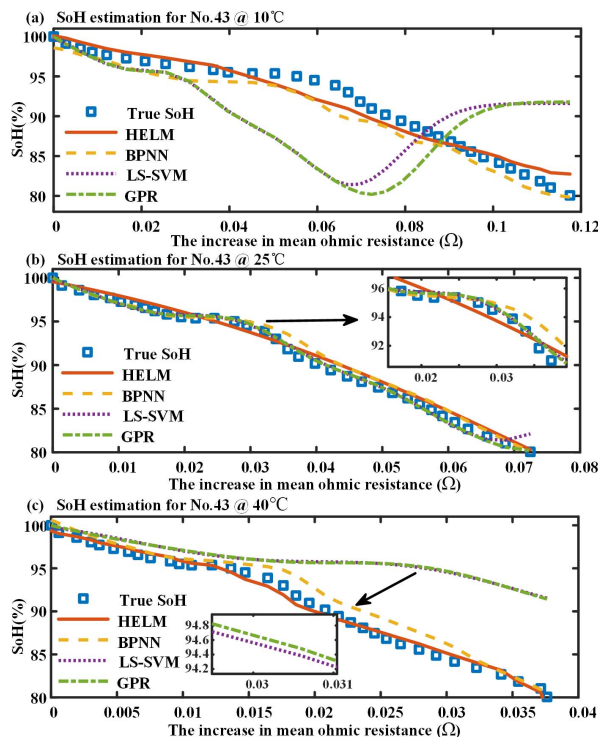


Fig. 10. SoH estimation trajectories of four ML algorithms (No. 43) at three different temperatures at (a) 10 °C, (b) 25 °C, and (c) 40 °C.

AE and RMSE of the HELM are the least among all four algorithms in these scenarios, which means that the HELM achieves a good balance between estimation accuracy and stability, and it has a superior ability of generalization. When the training sample and the testing sample are from the same temperature of 25 °C [Fig. 10(b)], the SoH estimation results of four algorithms all track the true SoH values efficiently. The GPR and LS-SVM show the very strong ability of regression under this circumstance, and their maximum errors are much smaller than those of HELM and BPNN (Table IX), which indicates that the GPR and LS-SVM can achieve high accuracy when the battery test sample has similar input characteristics with training sample. Although the accuracy of the HELM is not all the highest in these comparative tests, it shows a good performance of achieving stable accuracy at three different temperatures.

TABLE VIII
CONFIGURATIONS OF FOUR ML ALGORITHMS

Algorithm	Configurations
HELM	Number of hidden layers = 2, Number of hidden neurons = 20, Activation function= Sigmoid
BPNN	Number of hidden layers = 2, Number of hidden neurons = 20, Learning rate = 0.03, EPOCHS=500, Transfer function= Tansig and Purelin
LS-SVM	Kernel function = RBF, Parameter optimization function = Grid search
GPR	Covariance function = Squared exponential, Likelihood function = Gaussian, Inference method = Exact

TABLE IX
SoH ESTIMATION PERFORMANCE OF FOUR ML ALGORITHMS AT THREE DIFFERENT TEMPERATURES

Training sample	Testing sample	Method	Estimation conditions		Average training time (s)	Maximum AE (%)	MAE (%)	RMSE (%)
@10°C	No. 43 @10°C	HELM	0.0117	2.81	1.33	1.8852		
		BPNN	0.1897	3.66	1.47	1.9450		
		LS-SVM	0.0012	11.79	5.21	6.7601		
		GPR	0.0312	12.03	5.75	7.0781		
	No. 42 @25°C	HELM	0.0098	1.02	0.65	0.6913		
		BPNN	0.1459	1.87	0.69	0.5215		
@25°C	No. 43 @25°C	LS-SVM	0.0021	0.85	0.30	0.3553		
		GPR	0.0256	0.61	0.28	0.3233		
		HELM	0.0087	1.59	0.97	0.6245		
	No. 43 @40°C	BPNN	0.1760	2.33	1.15	1.9698		
		LS-SVM	0.0015	11.38	4.85	6.3213		
		GPR	0.0304	11.37	4.89	6.2793		

From the perspective of elapsed time, the training speed of HELM is second only to the LS-SVM (Table IX). Although the network structures of HELM and BPNN are similar, the training process of HELM is much faster than that of BP, benefiting from the random assignment of hidden neuron parameters. Another feature of HELM is that it only needs to avoid overfitting by solving regularization and instead of optimizing the hyperparameters, such as LS-SVM and GPR. Therefore, HELM can get a more efficient training process than other ML methods when optimization problems are taken into consideration, especially the data volume is large [36].

In summary, the SoH estimation results in the condition of different batteries at the same temperature, the different range of MOR for batteries, and different batteries at different temperatures show that the HELM has a good generalization ability, and the estimation results of the proposed framework are accurate and robust. The HELM framework effectively deals with input HI from different temperatures effectively and establishes the mapping relationship between HI and capacity in a randomly assigned way. These characteristics allow the HELM framework free for artificial adjustment for different batteries and different working conditions.

V. CONCLUSION

In this research, a synergy of the unique HI (the increase in MOR) with an HELM has been exploited to produce a correlation-based and HELM-oriented framework for online SoH estimation. The HI can be derived online based on the Thevenin model and using the FFRLS algorithm, and the experimental tests have proved that it is insensitive to the change of different loading profiles and can characterize the degraded capacity effectively in dynamic conditions. The HELM is introduced to develop the online SoH estimation framework, which has been evaluated from two perspectives: 1) the HELM-oriented framework has been verified by contrastive SoH estimation with BPNN, LS-SVM, and GPR and 2) the framework has been further validated using battery data from different temperatures. Experimental results indicate that the HELM enabled the framework to perform stably with the outstanding generalization ability and tuning-free characteristic. In the case of using one battery for training, the well-trained HELM combining the effective HI can be directly used to accurately estimate the SoH of other batteries with different loading profiles and different aging temperatures.

The developed techniques and results presented in this article provide guidance for SoH online estimation on the BMS, especially for implementation in real EVs scenarios with dynamic loading conditions and varying temperatures. The future work could consider the SoH estimation compensation at a lower temperature to overcome the bottleneck of unsatisfactory performance at 10 °C and further expand the applicability of the proposed framework to more applicable conditions.

APPENDIX

A. Code Availability

Code for the data processing is available at the website: https://personal.ntu.edu.sg/egbhuang/elm_codes.html. Also, the more details of modeling work are available from Huang Guangbin's personal page.

REFERENCES

- [1] M. Berecibar, I. Gandiaga, I. Villarreal, N. Omar, J. Van Mierlo, and P. Van den Bossche, "Critical review of state of health estimation methods of Li-ion batteries for real applications," *Renew. Sustain. Energy Rev.*, vol. 56, pp. 572–587, Apr. 2016.
- [2] L. Zheng, L. Zhang, J. Zhu, G. Wang, and J. Jiang, "Co-estimation of state-of-charge, capacity and resistance for lithium-ion batteries based on a high-fidelity electrochemical model," *Appl. Energy*, vol. 180, pp. 424–434, Oct. 2016.
- [3] M. A. Hannan, M. S. H. Lipu, A. Hussain, and A. Mohamed, "A review of lithium-ion battery state of charge estimation and management system in electric vehicle applications: Challenges and recommendations," *Renew. Sustain. Energy Rev.*, vol. 78, pp. 834–854, Oct. 2017.
- [4] J. Remmlinger, M. Buchholz, M. Meiler, P. Bernreuter, and K. Dietmayer, "State-of-health monitoring of lithium-ion batteries in electric vehicles by on-board internal resistance estimation," *J. Power Sources*, vol. 196, no. 12, pp. 5357–5363, 2011.
- [5] M. Dubarry and B. Y. Liaw, "Identify capacity fading mechanism in a commercial LiFePO₄ cell," *J. Power Sources*, vol. 194, pp. 541–549, Oct. 2009.
- [6] S. Zhang, X. Guo, X. Dou, and X. Zhang, "A rapid online calculation method for state of health of lithium-ion battery based on Coulomb counting method and differential voltage analysis," *J. Power Sources*, vol. 479, Dec. 2020, Art. no. 228740.
- [7] M. Galeotti, L. Cinà, C. Giannamico, S. Cordiner, and A. Di Carloac, "Performance analysis and SOH (state of health) evaluation of lithium polymer batteries through electrochemical impedance spectroscopy," *Energy*, vol. 89, pp. 678–686, Sep. 2015.
- [8] H. Pan, Z. Lü, H. Wang, H. Wei, and L. Chen, "Novel battery state-of-health online estimation method using multiple health indicators and an extreme learning machine," *Energy*, vol. 160, pp. 466–477, Oct. 2018.
- [9] W. Waag, C. Fleischer, and D. U. Sauer, "Critical review of the methods for monitoring of lithium-ion batteries in electric and hybrid vehicles," *J. Power Sources*, vol. 258, pp. 321–339, Jul. 2014.
- [10] D. Andre, C. Appel, T. Soczka-Guth, and D. U. Sauer, "Advanced mathematical methods of SOC and SOH estimation for lithium-ion batteries," *J. Power Sources*, vol. 224, pp. 20–27, Feb. 2013.
- [11] N. T. Tran, A. B. Khan, and W. Choi, "State of charge and state of health estimation of AGM VRLA batteries by employing a dual extended Kalman filter and an ARX model for online parameter estimation," *Energies*, vol. 10, p. 137, Jan. 2017.
- [12] S. Li, S. Pischinger, C. He, L. Liang, and M. Stapelbroek, "A comparative study of model-based capacity estimation algorithms in dual estimation frameworks for lithium-ion batteries under an accelerated aging test," *Appl. Energ.*, vol. 212, pp. 1522–1536, Feb. 2018.
- [13] I.-S. Kim, "A technique for estimating the state of health of lithium batteries through a dual-sliding-mode observer," *IEEE Trans. Power Electron.*, vol. 25, no. 4, pp. 1013–1022, Apr. 2010.
- [14] P. Shen, M. Ouyang, L. Lu, J. Li, and X. Feng, "The co-estimation of state of charge, state of health, and state of function for lithium-ion batteries in electric vehicles," *IEEE Trans. Veh. Technol.*, vol. 67, no. 1, pp. 92–103, Jan. 2018.
- [15] X. Bian, L. Liu, J. Yan, Z. Zou, and R. Zhao, "An open circuit voltage-based model for state-of-health estimation of lithium-ion batteries: Model development and validation," *J. Power Sources*, vol. 448, Feb. 2020, Art. no. 227401.
- [16] D. Liu, J. Zhou, H. Liao, Y. Peng, and X. Peng, "A health indicator extraction and optimization framework for lithium-ion battery degradation modeling and prognostics," *IEEE Trans. Syst., Man, Cybern. Syst.*, vol. 45, no. 6, pp. 915–928, Jun. 2015, doi: [10.1109/TSMC.2015.2389757](https://doi.org/10.1109/TSMC.2015.2389757).
- [17] R. Xiong, J. Tian, H. Mu, and C. Wang, "A systematic model-based degradation behavior recognition and health monitoring method for lithium-ion batteries," *Appl. Energy*, vol. 207, pp. 372–383, Dec. 2017.
- [18] Z. Chen, C. C. Mi, Y. Fu, J. Xu, and X. Gong, "Online battery state of health estimation based on genetic algorithm for electric and hybrid vehicle applications," *J. Power Sources*, vol. 240, pp. 184–192, Oct. 2013.
- [19] C. Weng, X. Feng, J. Sun, and H. Peng, "State-of-health monitoring of lithium-ion battery modules and packs via incremental capacity peak tracking," *Appl. Energy*, vol. 180, pp. 360–368, Oct. 2016.
- [20] L. Wang, C. Pan, L. Liu, Y. Cheng, and X. Zhao, "On-board state of health estimation of LiFePO₄ battery pack through differential voltage analysis," *Appl. Energy*, vol. 168, pp. 465–472, Apr. 2016.
- [21] G.-W. You, S. Park, and D. Oh, "Real-time state-of-health estimation for electric vehicle batteries: A data-driven approach," *Appl. Energy*, vol. 176, pp. 92–103, Aug. 2016.
- [22] H.-T. Lin, T.-J. Liang, and S.-M. Chen, "Estimation of battery state of health using probabilistic neural network," *IEEE Trans. Ind. Informat.*, vol. 9, no. 2, pp. 679–685, May 2013.
- [23] A. Nuhic, T. Terzimehic, T. Soczka-Guth, M. Buchholz, and K. Dietmayer, "Health diagnosis and remaining useful life prognostics of lithium-ion batteries using data-driven methods," *J. Power Sources*, vol. 239, pp. 680–688, Oct. 2013.

- [24] D. Yang, Y. Wang, R. Pan, R. Chen, and Z. Chen, "State-of-health estimation for the lithium-ion battery based on support vector regression," *Appl. Energy*, vol. 227, pp. 273–283, Oct. 2018.
- [25] J. Qu, F. Liu, Y. Ma, and J. Fan, "A neural-network-based method for RUL prediction and SOH monitoring of lithium-ion battery," *IEEE Access*, vol. 7, pp. 87178–87191, Jun. 2019.
- [26] R. R. Richardson, M. A. Osborne, and D. A. Howey, "Gaussian process regression for forecasting battery state of health," *J. Power Sources*, vol. 357, pp. 209–219, Jul. 2017.
- [27] L. Ungurean, M. V. Micea, and G. Cârstoiu, "Online state of health prediction method for lithium-ion batteries, based on gated recurrent unit neural networks," *Int. J. Energy Res.*, vol. 44, no. 8, pp. 6767–6777, Jun. 2020.
- [28] G.-B. Huang, M.-B. Li, L. Chen, and C.-K. Siew, "Incremental extreme learning machine with fully complex hidden nodes," *Neurocomputing*, vol. 71, nos. 4–6, pp. 576–583, 2008.
- [29] X. Hu, S. Li, and H. Peng, "A comparative study of equivalent circuit models for Li-ion batteries," *J. Power Sources*, vol. 198, pp. 359–367, Jan. 2012.
- [30] A. Farmann and D. U. Sauer, "Comparative study of reduced order equivalent circuit models for on-board state-of-available-power prediction of lithium-ion batteries in electric vehicles," *Appl. Energy*, vol. 225, pp. 1102–1122, Sep. 2018.
- [31] H. Pan, Z. Lü, J. Li, and L. Chen, "Estimation of lithium-ion battery state of charge based on grey prediction model-extended Kalman filter," *Trans. China Electrotech. Soc.*, vol. 32, pp. 1–8, Nov. 2017.
- [32] B. Saha, K. Goebel, S. Poll, J. Christoffersen, and K. Goebel, "An integrated approach to battery health monitoring using Bayesian regression and state estimation," in *Proc. IEEE Autotestcon*, Sep. 2007, pp. 646–653.
- [33] L. Chen, Z. Lü, W. Lin, J. Li, and H. Pan, "A new state-of-health estimation method for lithium-ion batteries through the intrinsic relationship between ohmic internal resistance and capacity," *Measurement*, vol. 116, pp. 586–595, Feb. 2018.
- [34] G.-B. Huang, Q.-Y. Zhu, and C.-K. Siew, "Extreme learning machine: Theory and applications," *Neurocomputing*, vol. 70, nos. 1–3, pp. 489–501, 2006.
- [35] G.-B. Huang, L. Chen, and C.-K. Siew, "Universal approximation using incremental constructive feedforward networks with random hidden nodes," *IEEE Trans. Neural Netw.*, vol. 17, no. 4, pp. 879–892, Jul. 2006.
- [36] J. Tang, C. Deng, and G.-B. Huang, "Extreme learning machine for multilayer perceptron," *IEEE Trans. Neural Netw. Learn. Syst.*, vol. 27, no. 4, pp. 809–821, Apr. 2016.
- [37] A. Beck and M. Teboulle, "A fast iterative shrinkage-thresholding algorithm for linear inverse problems," *SIAM J. Imag. Sci.*, vol. 2, no. 1, pp. 183–202, 2009.
- [38] L. Chen, B. Tian, W. Lin, B. Ji, J. Li, and H. Pan, "Analysis and prediction of the discharge characteristics of the lithium-ion battery based on the grey system theory," *IET Power Electron.*, vol. 8, no. 12, pp. 2361–2369, Dec. 2015.
- [39] M. Ouyang *et al.*, "Low temperature aging mechanism identification and lithium deposition in a large format lithium iron phosphate battery for different charge profiles," *J. Power Sources*, vol. 286, pp. 309–320, Jul. 2015.



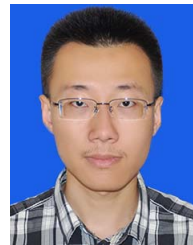
Lin Chen received the M.S. degree in computer applied technology from Guangxi University, Nanning, China, in 2004, and the Ph.D. degree in biomedical engineering from the Huazhong University of Science and Technology, Wuhan, China, in 2008.

Since 2011, she has been a Professor with the College of Mechanical Engineering, Guangxi University. She has hosted and participated in as many as ten national or regional fund projects. She has authored or coauthored more than 50 technical articles and holds more than 20 patents. Her research interests include automation and control, robotics, digital signal detection and processing, ac servo drives, battery management technology, and other related research work.



Yunhui Ding is currently pursuing the M.S. degree in mechanical engineering with Guangxi University, Nanning, China.

His research interest includes battery management systems in electric vehicles.



Huimin Wang received the bachelor's degree from the School of Mechatronics Engineering, Harbin Institute of Technology, Harbin, China, in 2016, and the M.S. degree in mechatronics engineering from Guangxi University, Nanning, China, in 2019. He is currently pursuing the Ph.D. degree in mechatronics engineering with the School of Mechanical Engineering and Automation, Harbin Institute of Technology, Shenzhen, China.

His research interest includes battery management systems in electric vehicles.



Yijue Wang received the M.Sc. degree in statistics from the University of Connecticut, Storrs, CT, USA, in 2017, where he is currently pursuing the Ph.D. degree in computer science.

Since 2015, he has worked on risk prediction problem with statistical analysis and machine learning algorithm with USA Insurance Company and Pharmacy Company. He has worked on different projects about closest pair algorithm and membership privacy with deep learning model as a research assistant. His research interests include membership attack learning models, closest pair algorithms, and battery

protection in machine learning models, closest pair algorithms, and battery management.



Bohao Liu is currently pursuing the M.S. degree in mechanical engineering with Guangxi University, Nanning, China.

His research interest includes battery management system in electric vehicles.



Shuxiao Wu is currently pursuing the M.S. degree in mechanical engineering with Guangxi University, Nanning, China.

His research interest includes battery management systems in electric vehicles

Hao Li, photograph and biography not available at the time of publication.



Haihong Pan received the Ph.D. degree in mechanical engineering from the Huazhong University of Science and Technology, Wuhan, China, in 2007.

Since 2008, he has been a Professor with the College of Mechanical Engineering, Guangxi University, Nanning, China. He has hosted and participated in as many as 16 national or regional fund projects. He has authored or coauthored more than 60 technical articles and has been granted with more than 50 patents. His research interests include electromechanical control theory and method of complex electromechanical systems, all digital networked ac servo drive motor control theory and technology, and other related research work.